Journal of the European Ceramic Society 22 (2002) 1711–1721

www.elsevier.com/locate/jeurceramsoc

Cerium (IV) oxide synthesis and sinterable powders prepared by the polymeric organic complex solution method

Pedro Durán*, Francisco Capel, Dionisio Gutierrez, Jesús Tartaj, Carlos Moure

Instituto de Cerámica y Vidrio (CSIC), Electroceramics Department, 28500-Arganda del Rey, Madrid, Spain

Received 20 June 2001; accepted 13 October 2001

Abstract

Three processing methods making use of different cations complexant as citric acid (CA), polyvinylalcohol (PVA) or polyethylene glycol (PEG) have been used to prepare high purity fine CeO_2 powder with different particle size and agglomeration degrees. Green compacts prepared from the differently agglomerated powders were studied by Hg-porosimetry, and pore-size distribution curves were taken to compare the uniformity of the green compacts microstructure. The citrate-based prepared powders could be sintered to densities of 98% of theoretical at 1250 °C for 10 h, and to nearly fully dense (99.5% theoretical) at 1380 °C for 1 h. Otherwise, sintering temperatures of 1380 °C and $\geqslant$1650 °C were necessary to obtain densities of $\approx$98% theoretical when using PEG and PVA as complexant, respectively. The different shrinkage-rate behavior was assumed to be closely related to differences in the pore-size distribution in the green compacts. Pore-size evolution was taken into account to study the microstructural development during sintering. Moderate grain growth (grain size $\approx$200 nm) was observed until densities lower than about 90% theoretical, while it considerably increases for higher densities. Grain size and microstructure uniformity could be related to the green compacts uniformity, i.e. the pore-size distribution and the agglomeration degree.

Keywords: CeO_2; Microstructure-final; Powders-chemical preparation; Precursors-organic; Sintering

1. Introduction

Ceria, contrarily to zirconia and bismuth oxide in which several polymorphic transformations are to be present in different temperature ranges, has the fluorite structure which is stable from room temperature up to its melting point. On the other hand, ceria easily form extensive solid solutions with several alkaline and rare-earth oxides maintaining the stable fluorite structure. The lower valences of the dopant cations are charge compensated by the introduction of mobile oxygen vacancies.[1,2] Dense doped cerias solid solutions have demonstrated to be of considerable interest not only like solid electrolytes in SOFC devices[3] but also as catalytic supports.[4] Dense ceramic membranes are needed for electrolytes and for some anode applications, but it is very difficult to achieve dense ceria bodies by conventional techniques at relatively low sintering temperatures ($<$1500 °C) in air,[5] at least without additives. For example, it was reported that dense CeO_2 ceramic bodies with additives could be obtained at sintering temperatures lower than 1500 °C[6] and, on the other hand, pure CeO_2 undergoes reduction at high temperatures.[5] Therefore, sinterable powders are required for the fabrication of dense CeO_2-based ceramics at low temperature.

Recently, there have been great efforts in the preparation of sinterable CeO_2 powders. Chen and Chen[7] prepared CeO_2 powders by aging a cerium (III) nitrate solution in the presence of hexamethylentetramine. The as obtained CeO_2 powders could be sintered to almost full density at temperatures as low as 1250 °C. Zhow et al.[8] achieved highly sinterable CeO_2 powders by the electrochemical synthesis method, and dense bodies ($\geqslant$ 99.8% theoretical) with a grain size of about 0.35 μm were obtained at 1300 °C. The hydrothermal synthesis method was used by Hirano and Kato[9,10] to prepare nanocrystalline CeO_2 powders with different morphologies and sinterabilities. Nakane et al.[11] attained full density CeO_2 ceramics at 1150 °C by using the hydrazine preparation method. Powder morphology, particle size, and pore size distribution in the green compacts were the main parameters taken into account to explain

* Corresponding author. Tel.: +34-91-871-1800; fax: +34-91-870-0550.

E-mail address: pduran@icv.csic.es (P. Durán).

0955-2219/02/$ - see front matter
PII: S0955-2219(01)00483-6

the sintering behaviour and the microstructure evolution in fine CeO_2 powders.[12,13]

New approaches in the preparation of fine oxide powders are emerging in the last years.[14–18] These are based on the Pechini-type process, i.e. the in situ polymerizable complex (IPC) method or the another type of polymer complex solution (PCS) method which, in principle could overcome some disadvantages of the IPC method. The IPC method has an important advantage over the above mentioned ones such as a better compositional homogeneity but a strong disadvantage as is the effective removal of large amounts of organic material. On the other side, the PCS method is a simpler organic polymer gel one which differs from the IPC technique in that it utilizes water as a solvent instead of organic solvents.

In the present work we carried out a comparative study of the powder characteristics and its sintering behaviour on CeO_2 powders obtained by both the IPC and PCS methods. For comparison, a CeO_2 powder prepared by a polyethylene glycol-based process (PEG-method) was also carried out for the synthesis of the same material.

2. Experimental procedure

In all the cases, the IPC, PCS, and PEG organic polymer methods, cerium nitrate hexahydrate ($Ce(NO_3)_3{\cdot}6H_2O$) 99.99% pure (Alfa Products, Karlsruhe, Germany) was used as source of Ce. While the anhydrous citric acid (CA), ($C_6H_8O_7$, E. Merk, Darmstad, Germany) as a complexant and ethylene glycol (EG), ($C_2H_6O_2$, E. Merk, Darmstad, Germany) as a solvent were required in the IPC method, a simple polyvinylalcohol (PVA) with an averaged molecular weight of 8000—10,000 and pure water as complexant and solvent respectively, were used in the PCS route. Finally, a polyethylene glycol, ($(C_2H_6O_2)_n$, E. Merk, Darmstad, Germany) with an average molecular weight of 200 and water were used in the PEG method.

The same amount of $Ce(NO_3)_3{\cdot}6H_2O$ (0.1 mol) was used in the distinct chemical routes which was dissolved in the necessary amount of water. This transparent solution was then mixed with (1) the required amount of an organic solution containing EG and CA in a molar ratio of 4:1, (2) a solution containing 0.01 mol of PVA dissolved in 1000 g of water, and (3) a solution containing 0.1 mol of PEG dissolved in 1000 g of water, in the case of IPC, PCS, and PEG methods, respectively. A typical flow chart for the three synthesis methods is shown in Fig. 1(A)–(C).

The different prepared powder precursors, hereinafter labeled as PECH, PVA, and PEG samples, were calcined at 650 °C for 2 h and attrition milled with zirconia ball media in methanol for 2 h. After milling, the nanocrystalline CeO_2 powders were characterized by X-ray diffraction (XRD), and transmission electron microscopy (Hitachi, H-7000 model, 125 KV, Shinjuku-Ku, Tokyo, Japan). X-ray diffraction patterns were obtained with a diffractometer (Siemens D-5000, Erlangen, Germany) using nickel-filtered CuK_α radiation. The crystallite size (D) was calculated using for several diffraction lines from the Scherrer formula.

$$D = 0.9\lambda/\beta\cos\theta$$

Where λ is the wavelength of X-rays, β the corrected half-width that is obtained using the (111) line of the pure silicon as the standard. Specific surface areas of the milled CeO_2 powders were measured by the Brunahuer–Emmett–Teller (BET) method (Quantachrome MS-16 model, Syosset, NY), using nitrogen as an absorbate after drying under vacuum. From the data of specific surface areas, the particle sizes were calculated using the equation:

$$\phi = 6/S\rho$$

where ϕ is the average diameter of spherical particle, S the surface area of the powder, and ρ the theoretical density of CeO_2 (7.132 g/cm^3).

Calcined and granulated powders were cold isopressed at 200 MPa. Pore size distributions of as pressed compacts were determined by mercury penetration porosimetry (Micromeritics, Autopore II, 9215, Norgross, USA). Sintering was performed in air using a constant heating rate of 5 °C/min up to 1500 °C in a dilatometer (Netzsch 402E of Geratebau, Bayern, Germany) which allowed continuously monitoring of the shrinkage kinetics. The samples were also sintered isothermally at 1250 and 1380 °C. The density of the samples after sintering was measured by the Archimedes method.

The microstructure of sintered samples was examined in a scanning electron microscope (Zeiss DSM 950, Oberkochem, Germany). The grain size was measured by the line intercept method on the polished and thermally etched sintered samples.

3. Results

3.1. Powder characterization

The powder synthesized by either of the used routes was identified by X-ray diffraction to be cerium oxide with the cubic fluorite structure. The measured lattice parameter "a" was 0.5411 ± 0.0005 nm which is closed to the report value (0.5415 nm).[11] Fig. 2 shows XRD patterns of powders prepared by the PEG method heat-treated at different temperatures.

Transmission electron micrographs of the powders are shown in Fig. 3(a–c). The morphology of the particles is

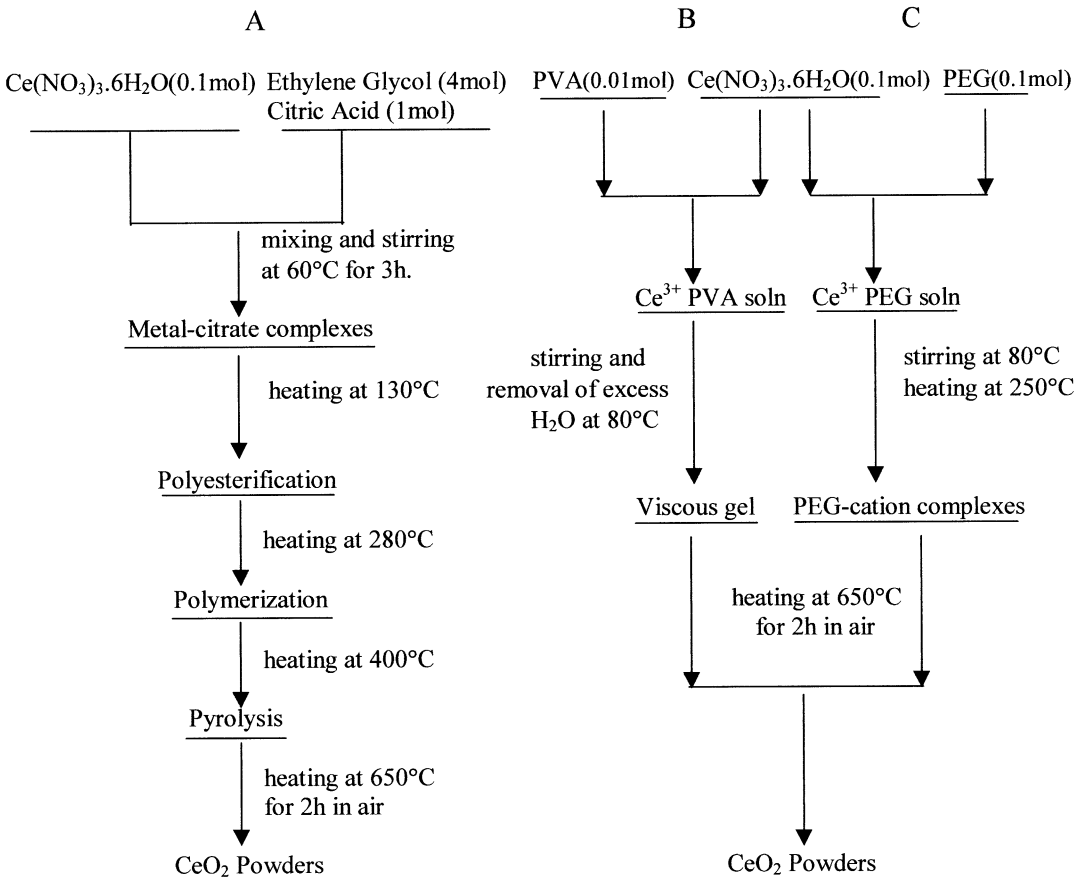

Fig. 1. Flow chart for preparing CeO_2 by the modified Pechini method (A), the PVA-based method (Mw of PVA = 8000–10,000) (B), and by the PEG method (Mw of PEG = 200) (C).

very similar in all of them and the only difference is the agglomeration degree which varied in the sense PECH < PEG < PVA, CeO_2 powders. The cation distribution in the PECH-cation, PEG-cation, and PVA-cation complexes could be the cause for the different agglomeration levels.

Table 1 summarizes the main characteristics of the different powders prepared at the present experimental conditions. The particle sizes fall between 8 and 15 nm in the case of the PECH and PEG powders, which agrees well with the average size (between 7.5 and 11.5 nm) obtained by the X-ray line broadening method. The specific surface areas measured by the BET method were 65 and 99 m^2/g, and the calculated particle size from them 12.5 and 8.5 nm for PECH and PEG CeO_2 powders, respectively, indicate that all the particles are almost spherical and weakly agglomerated. This is not the case of the PVA CeO_2 powders in which hard agglomerates between faceted particles was its main characteristic. On the other hand, the BET specific surface area of this CeO_2 powders was as low as 8.5 m^2/g.

Table 1
Characteristics of CeO_2 calcined powders

Powder	BET surface area (m^2/g)	Particle size (nm)			
		TEM	XRLB	SEM	BET
PECH	65	13	11.5	>50	12.5
PEG	99	8	7.5	>50	8.5
PVA	8.5	>200	–	>200	≈100.0

3.2. Compaction behaviour

The compaction behaviour of the CeO_2 prepared powders is a crucial parameter for their sintering. On the other hand, the pore morphology also has a strong influence on the sintering behaviour of green compacts. Therefore, it is very interesting to compare the uniformity of the compaction for the different CeO_2 powders. SEM micrographs of the fracture surfaces of green compacts prepared from the different CeO_2 powders are shown in Fig. 4. The two powders PECH and PEG, having the higher specific surface areas, compacted quite uniformly to almost a same green density of 50 and 53% theoretical density, respectively. The PVA powders, having the lower specific surface area, compacted to the higher green density of 56% of theoretical density. Comparing these results with the pore volume of the different green compacts, it was found that the PVA

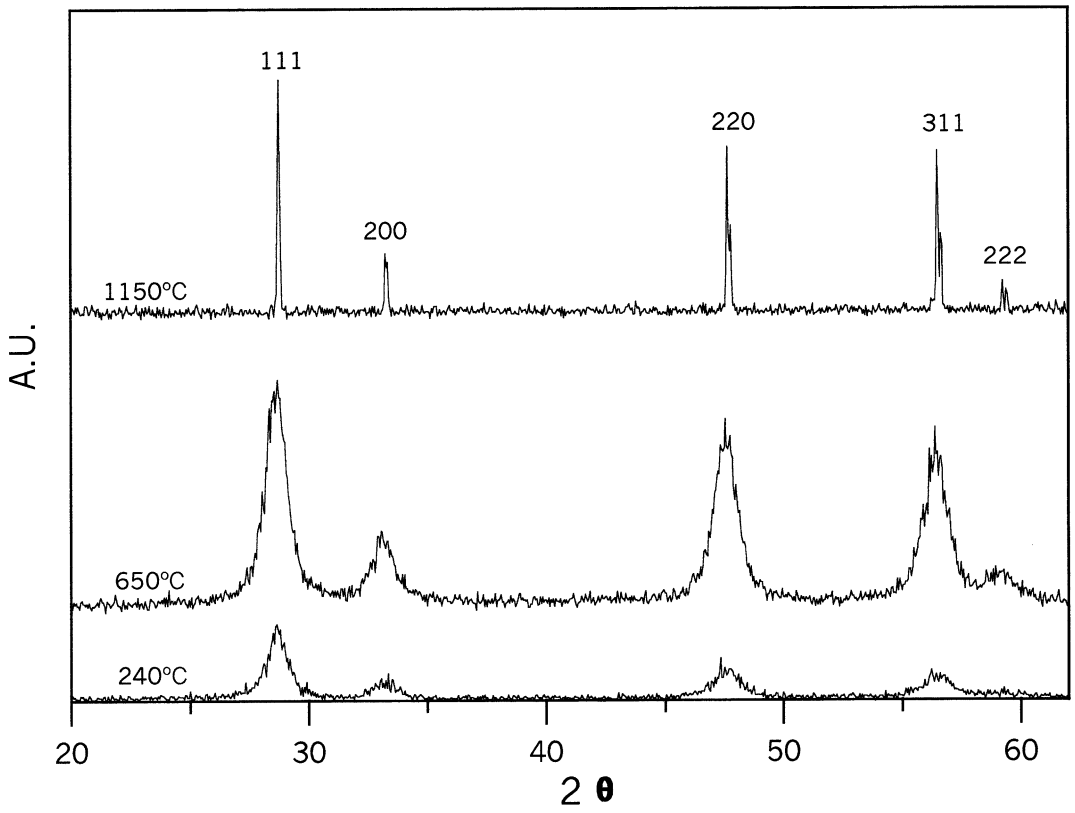

Fig. 2. X-ray diffraction patterns for CeO_2 powders prepared by the PEG method calcined at the indicated temperatures.

compact has the smallest pore volume (0.10 cm^3/g) and the PEG compact the largest (0.139 cm^3/g). The presence of pores with a diameter smaller than 8 nm is probably the cause for the higher pore volume of the PEG compacts. Density gradients are clearly seen in the PVA compacts with a heterogeneous packing powder.

Fig. 5 shows the pore-size distribution curve for the three kind of green compacts. As expected, the PECH compact has a very narrow and unimodal pore-size distribution with only a maximum centered at about 10 nm, which indicates that the major part of the porosity is present as an intraagglomerate porosity. The pore-size distribution of the PEG compact shows a maximum at a diameter of 15 nm and other two centered at about 8 and 4 nm. The higher one can be attributed to an interagglomerate porosity and the others at smaller pore diameter to the intraagglomerate porosity. The pore size distribution curve for the PVA compact demonstrates that the major part of the porosity is an interaglomerates one which present a maximum pore diameter at about 42 nm.

3.3. Sintering behaviour

The sinterability of the different CeO_2 powders is shown in Fig. 6, where the relative density is plotted against temperature. The PECH sample reaches an almost constant density of 99.4% of theoretical at about 1380 °C, whereas the PEG and PVA samples sintered to density values of 98 and 90% of the theoretical, respectively, at the same temperature. The densities after sintering at 1500 °C were 99.5, 98 and 92% of the theoretical for the PECH, PEG, and PVA samples, respectively.

An isothermal sintering study was also carried out, and Fig. 7 shows the obtained results for the different samples isothermally sintered at 1250 and 1380 °C. The highest relative density that was attained at 1250 °C was 98 and 97% of the theoretical after a heat-treatment of 10 h for PECH and PEG samples, respectively, whereas only about 85% of the theoretical was achieved for the PVA sample. Near full-density (99.4% of the theoretical) was attained for the PECH sample sintered at 1380 °C for only 1 h. In the case of the PEG sample a constant density value of 98% of the theoretical was achieved. The highest relative density that was attained for the PVA sample sintered at 1380 °C was 91% of the theoretical after prolonged firing. These whole of results indicate that the PECH powder has the higher sinterability.

The shrinkage and shrinkage rate of the different powder compacts measured by dilatometry are shown in Fig. 8. The end density is achieved at about 1400 °C for PECH and PEG samples. Densification of the PVA samples takes place over a relatively narrow temperature regime between 1400 and 1650 °C, Fig. 8(A). The PECH and PEG samples which can be considered as

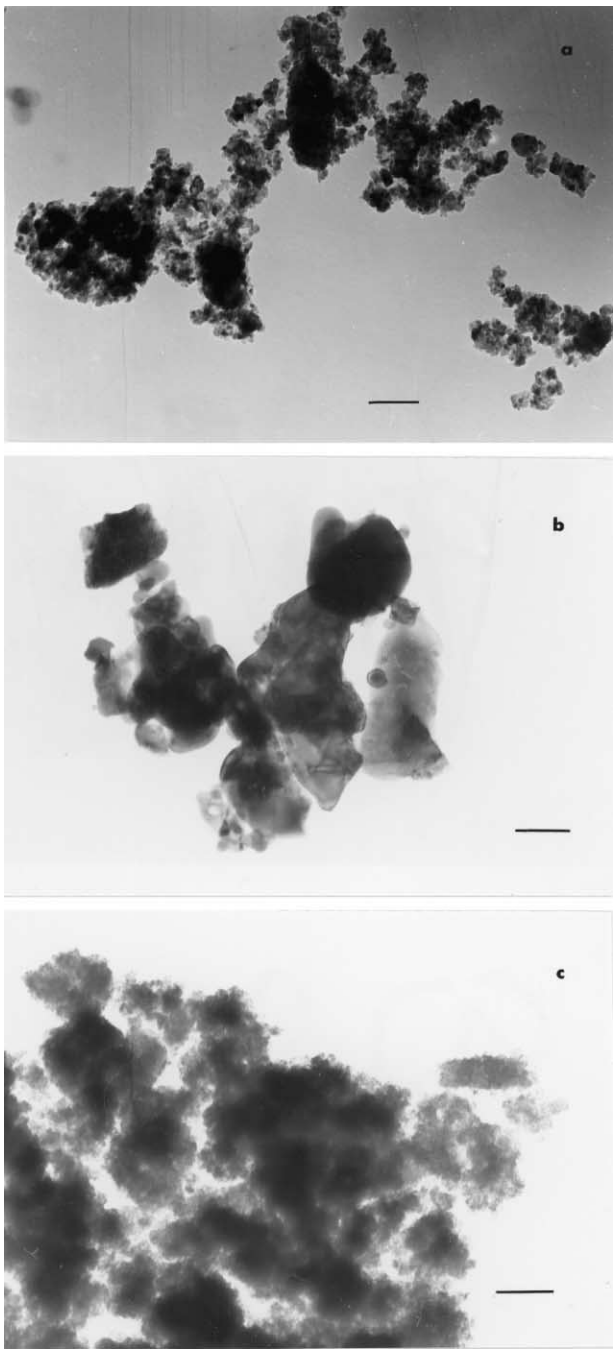

Fig. 3. TEM micrographs of calcined CeO_2 powders prepared by the Pechini method (a), the PVA-based method (b), and the PEG method (c). (Bar = 0.2 μm).

nanostructured green compacts started to shrink at temperatures as low as 400 °C, i.e. diffusion process become important at this temperature and densification could already be measurable. Fig. 8(B) shows the densification rate as a function of sintering temperature for the different prepared samples. As it can be observed, the temperature for the maximum densification rate was increased with increasing both the size of the most frequent pore size and the agglomeration degree. Thus, the temperatures of the main maximum densification rate

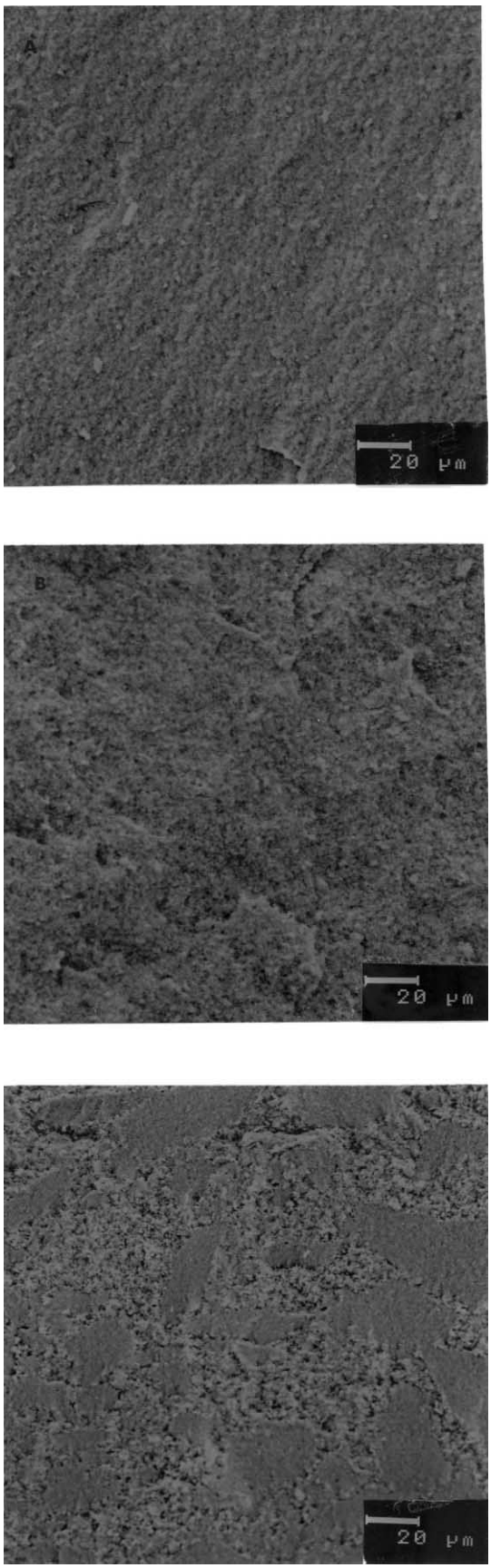

Fig. 4. SEM photomicrographs of green compacts fracture surfaces prepared by (A) Pechini, (B) PEG, and (C) PVA method.

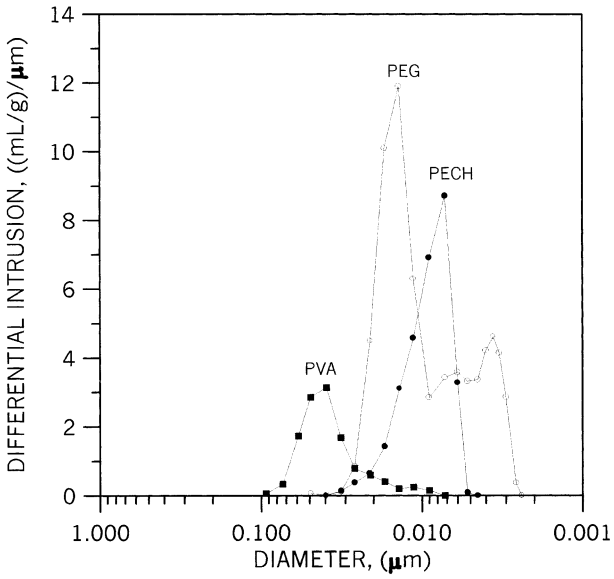

Fig. 5. Pore-size distribution curves for the differently prepared green powders compacts.

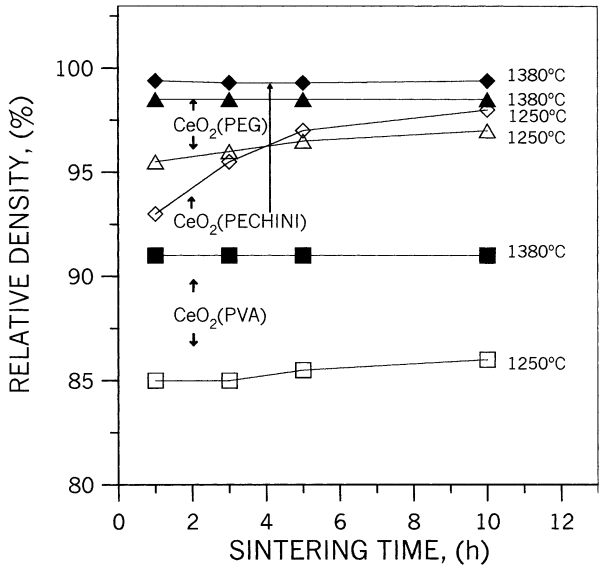

Fig. 7. Relative density versus time for the CeO_2 powders isothermally sintered at 1250 and 1380 °C.

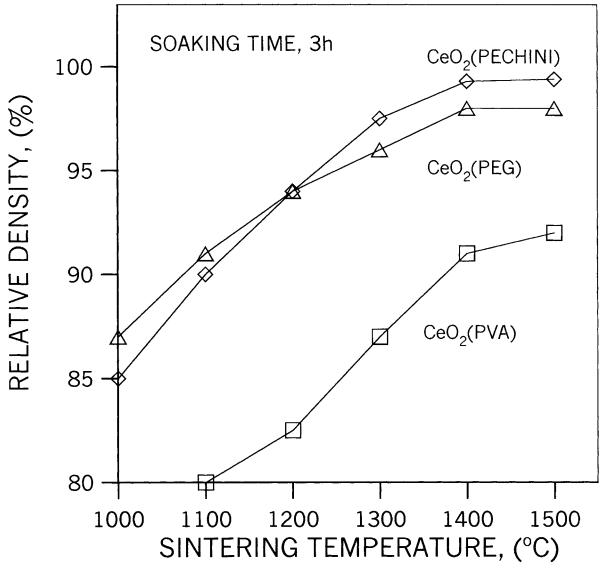

Fig. 6. Temperature dependence of the relative density after 3 h isothermal sintering for the different CeO_2 compacts.

were 1090, 1140 and 1510 °C for PECH, PEG, and PVA samples. It must be mentioned that a second maxima at 1060 and 1390 °C were also present for PEG, and PVA samples, respectively. These two maxima can be attributed to the elimination of the smaller pores

3.4. Microstructural evolution

To know the microstructural evolution of the PECH and PEG samples, a series of microstructures and pore size distributions at different densification levels were observed. The evolution of the pore size distributions is shown in Fig. 9. As can be seen, the smaller pores disappear and the larger grow, giving rise to a relative increase of the average pore size from 8 nm in the green compact to 12, 15 and 17 nm at 800, 900 and 1100 °C, respectively, [Fig. 9(A)]. As is shown in Fig. 10, the pore volume hardly changes until 600 °C, above that it rapidly decreases. It indicates that below 600 °C no relevant microstructural features took place. As is clearly seen from Fig. 9(A), as the relative density was increased from 62% at 800 °C to 88% at 1100 °C, fine pores existing in the green compact were eliminated and the average pore size shifted to a larger pore diameter. Therefore, it can be said that, pore growth dominated in the PECH compact for densities below 65%, and decreased for higher densities.

In the case of the PEG samples the pore volume curve has a similar shape to that of PECH (Fig. 10). However, as the relative density was increased the pore size distribution became narrower, and the average pore size increased at the beginning and decreased thereafter. On the other hand, the pore growth rate is also higher than in the PECH samples, i.e. from 12 nm in the green compact to 26 nm at 1100 °C [Fig. 9(B)].

Fig. 11 shows the SEM micrographs of the polished and thermally etched samples sintered at 1250 and 1380 °C. The grain sizes increases from 0.8, 3 and 1 μm at 1250 °C to about 2, 6 and 2 μm at 1380 °C for PECH, PEG, and PVA sintered samples. A particular feature was found in the case of the PVA sintered samples, [Fig. 11(C) and (F)]. These show evidence for a slower grain growth rate comparatively with those present in the PECH and PEG samples, which probably corresponded with different sintering stages.

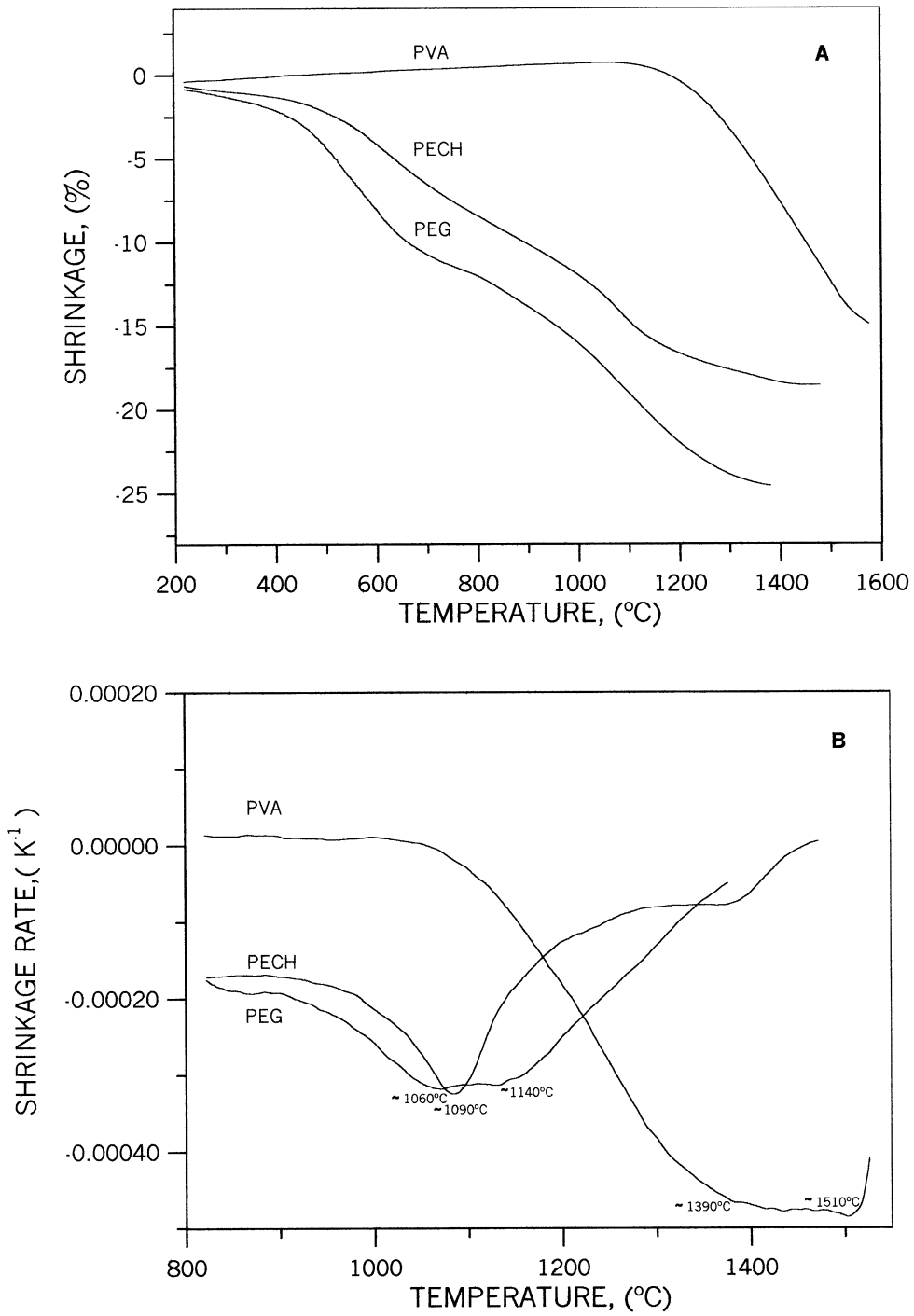

Fig. 8. Temperature dependence of linear shrinkage (A) and differential linear shrinkage (B) for the different CeO_2 compacts. The heating/cooling rate was 5 °C/min.

The relationship between grain size and sintered density for the PECH and PEG samples is shown in Fig. 12. It shows that the grain size increases slowly until a given relative density above which grains grow rapidly. Such a density value was located at about 90% relative density in the present study, although in the case of PEG samples the grain size for the highest density ($\geqslant$98% theoretical density) was comparatively higher (5 against 8 μm).

4. Discussion

In this paper we report a study on the preparation, characterization, and the sintering behaviour of CeO_2 powders with different agglomeration degrees. According to our sintering and microstructure results a close correlation between powder agglomeration, green compact characteristics, and the sintering behaviour exists.

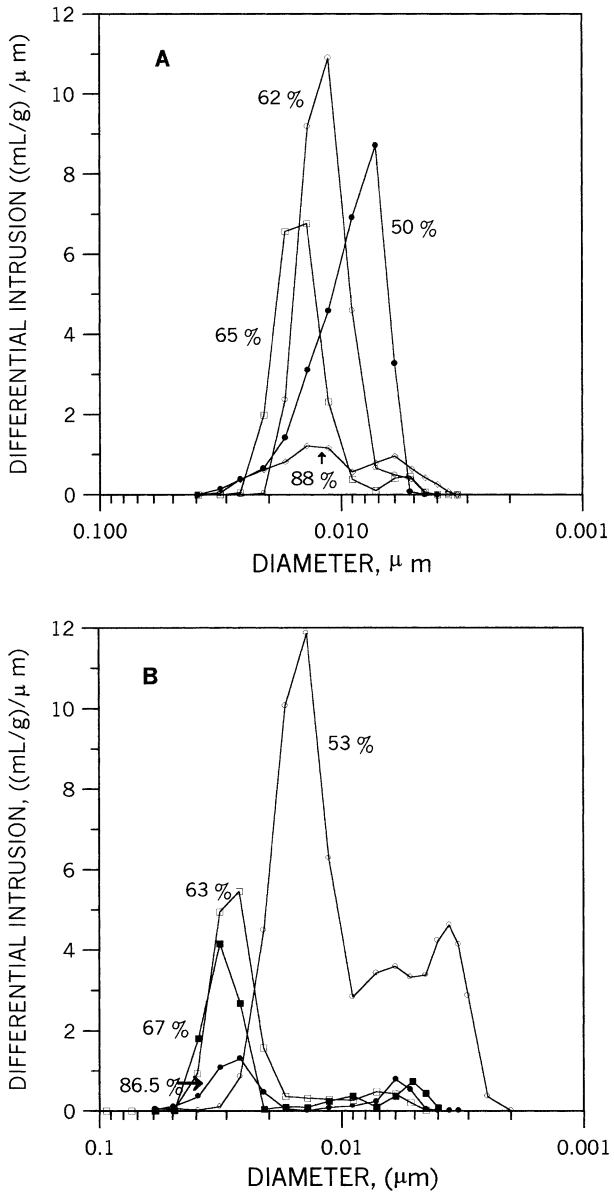

Fig. 9. Pore-size distributions of PECH (A) and PEG (B) compacts at various sintered relative densities (% theoretical density), showing the pore-size evolution during sintering.

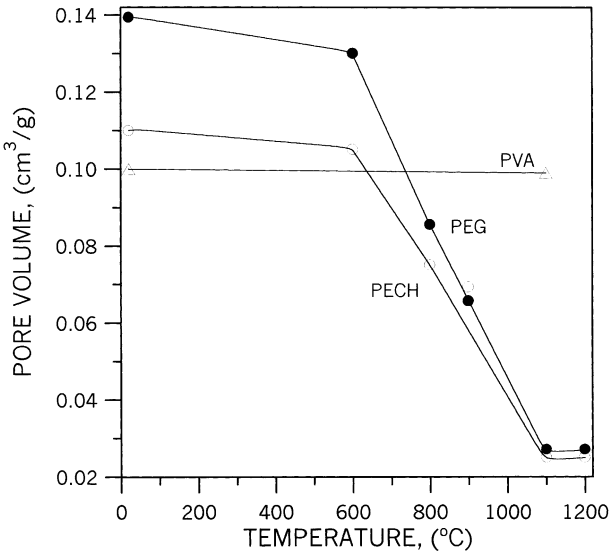

Fig. 10. Total pore volume versus sintering temperature for PECH, PEG, and PVA green compacts.

For example, the high internal porosity of a loose powder (almost agglomerate-free) as is the case of the PECH and PEG samples, leads to the consolidation in green compacts in which the most frequent pore-size is very similar and in the nanoscale (see Fig. 5). The maxima at 8 and 12 nm in the pore size distribution curves for PECH and PEG green compacts, respectively, indicate a homogeneously distributed porosity (better in the case of the PECH samples) that can be eliminated at low temperature. In the case of the PVA samples a broader pore size distribution curve, as a consequence of both a higher agglomeration degree and denser agglomerates, resulted in a lower sinterability (see Figs. 3 and 5). On the other hand, the green compacts of the PECH and PEG powders show a high-density and homogeneous packing of the particles, while the PVA green compacts have clear packing density gradients (Fig. 4). Those green compacts characteristics enhanced densification in the early stages of sintering (see Fig. 6), but the strong shrinkage required for almost full density in the case of the PEG samples could be considered as a disadvantage. Note that for the same sintering conditions, i.e. after sintering at 1380 °C for 2 h, the relative density of the PVA samples was only about 91% theoretical density.

From Fig. 6(A) and (B) two relevant features can be attained, (i) the improved sinterability of the PECH and PEG compacts is strongly related to the pore-size distribution, i.e. the smaller pore size and narrower pore-size distribution in green compacts enhanced the driving force for shrinkage of the pores and, therefore, a rapid and homogeneous densification, and (ii) there is a defined temperature to eliminate the pores with different sizes, i.e. the smaller ones are eliminated at a lower temperature and the larger ones need a higher temperature to be eliminated. This statement is consistent with the idea reported by Roseen et al.[19,20] that the smaller the size of the most frequent pore size in the green compact, the lower the temperature at which these pores were eliminated. On the other hand the retardation of densification in the case of PVA samples, having both the larger most frequent pore size and the higher agglomeration degree, supported the above contention. Although other factors affecting the densification rate could be considered,[21–23] the almost similar three densities at the maxima densification rate, 1090, 1140 and 1510 °C, that were 88.5, 91.5, and 92% of theoretical density for PECH, PEG, and PVA samples, respectively, allowed us to assume that both the pore size and

the agglomeration degree are the two dominant factors for the densification rate.

From Figs. 6 and 8 it is clear that significative densification starts at lower temperatures (≈ 600 °C) in the sample with smaller pore size fraction (between 4 and 8 nm), as is the case of the PEG powder samples, but the excessive grain growth at high temperature led to a final sintering density somewhat lower than that of the

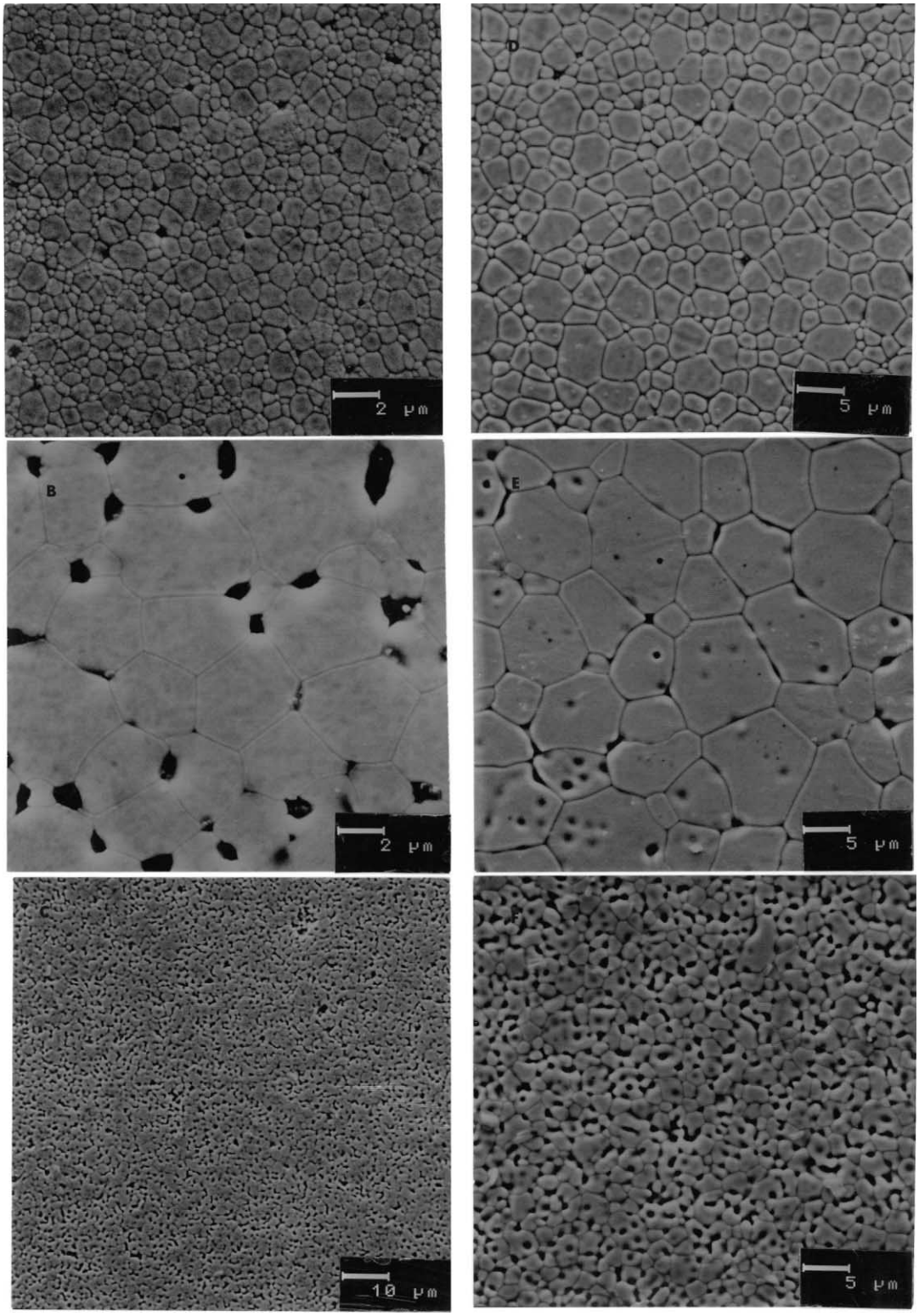

Fig. 11. SEM micrographs of polished and thermally etched sections of PECH, PEG, and PVA CeO_2 samples sintered at 1250 °C (A)–(C) and at 1380 °C (D)–(F).

PECH ones which have a similar initial particle size but with a narrower pore size distribution and lower agglomeration degree. This shows the importance of preventing or suppressing the grain growth during the sintering of nanostructured green compacts to take all the advantages of the high reactivity of nanoparticles. Densification of PVA samples which had an initial relatively small particle size of about 0.1 μm, but strongly agglomerated, began at temperatures above 1150 °C. Taking into account the inverse dependence on the fourth power of particle diameter,[24] it follows that the densification rate of PECH and PEG nanocristalline samples is, at least, 4 orders of magnitude greater than that for samples with 0.1 μm particle size. The fact that just above 600 °C densification began to be significant means that at such temperature the grain boundary diffusion becomes considerable to influence sintering.[22] Consistently, the small pores are eliminated and a relatively high growth of pores takes place (Fig. 9). According to these results it seems that a critical pore size is to exist in close agreement with Kingery et al. suggestions,[25] i.e. those pores smaller than the critical size are eliminated while those larger ones grow. All these phenomena take place between the end of the initial sintering stage and during the intermediate sintering stage.

Although densification begins at very low temperatures, as is shown in Fig. 12, moderate grain growth was observed in PECH samples until a density lower than about 90% theoretical density is reached. Grain size in CeO_2 PEG sintered samples increases more rapidly above that density value. The more uniformly packed and better green microstructure in PECH samples can explain the delay in the grain growth process. Comparing with PECH (0.2 μm) and PEG (0.5 μm) for a similar

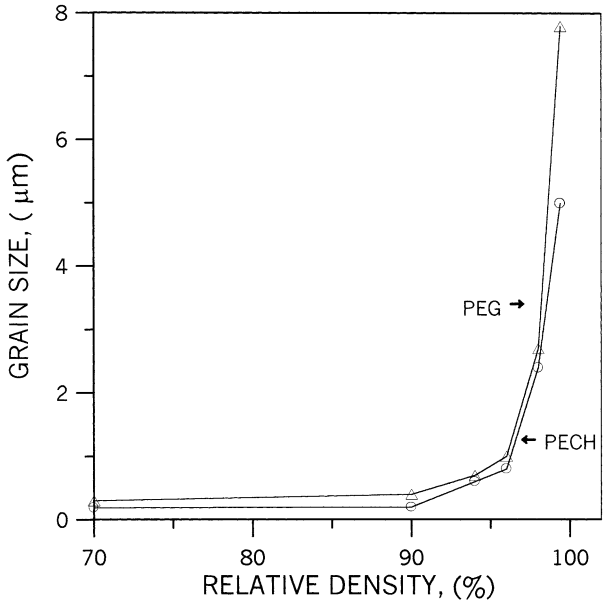

Fig. 12. Grain size as a function of density for PECH and PEG CeO_2 sintered samples.

densification level, in the case of the PVA sintered samples grain sizes as high as 2 μm were reached. The broader pore-size distribution, the high agglomeration level and, therefore, a heterogeneous green microstructure giving rise to density gradients on sintering were the main causes for its exaggerated grain growth.[26,27]

5. Conclusions

(1) Crystalline, almost agglomerate-free CeO_2 nanosized powders have been prepared by both the modified Pechini and PEG methods. When using PVA (Mw ≈ 8000—10,000) as complexant the prepared CeO_2 powders showed a high agglomeration degree.

(2) Green compacts having a fine uniform microstructure and narrow pore size distribution, with an average pore size on the order of the particle size, were consolidated in the case of the almost agglomerate-free powders. Heterogeneous green microstructure with density gradients and broad pore size distribution was present in the strongly agglomerated powder compacts.

(3) For the initial stage of sintering, the beginning of the densification showed a strong dependence on the pore size in the green compacts, and the smaller pores ($\leqslant$4 nm) disappeared at the lower temperatures ($\leqslant$600 °C) by surface diffusion processes with slight densification. Above that temperature, the maxima in the pore size distribution of the green compacts are closely related to the maxima in the densification rate.

(4) The smaller the size of the most frequent pore size in the green compacts the lower the sintering temperature, thus CeO_2 dense ceramic bodies ($\geqslant$ 98% theoretical density with submicrometer grain size) were obtained by sintering at 1250 °C in air for 10 h, and almost fully dense bodies (99.5% theoretical) at 1380 °C for 1 h, in the case of nonagglomerated powders. Higher temperatures, 1380 and 1650 °C, were needed to reach CeO_2 dense bodies (≈98% theoretical density) in the case of sintered samples having a higher agglomeration degree and a higher most frequent pore size in the green compacts.

(5) Although considerable grain growth occurred in the nearly dense sintered compacts ($\geqslant$1 μm relative to the original particle size of about 12 nm), but slight grain growth took place for densification levels below about 90% theoretical density maintaining the grain size nearly the nanoscale ($\leqslant$200 nm). Nonuniformity in the green microstructure led to a higher grain growth rate even at lower densification levels.

Acknowledgements

The present work was supported by the Spanish CICYT under contract: MAT-2000-815.

References

1. Kudo, T. and Obayashi, H., Oxygen ion conduction of the fluorite-type $Ce_{1-x}Ln_xO_{2-x/2}$. *J. Electrochem. Soc.*, 1975, **122**, 42–47.
2. Pascual, C., Jurado, J. R., Fernández, G., Del Olmo, L., Moure, C. and Durán, P., Electrical conductivity of solid solutions in the systems CeO_2–CaO and CeO_2–Ln_2O_3 (Ln = La, Nd, Sm, Gd, Er, Y). *Science of Ceramics*, 1983, **12**, 729–734.
3. Yahiro, H., Baba, Y., Egneli, K. and Arai, H., High temperature fuel cell with ceria–yttria solid electrolyte. *J. Electrochem. Soc.*, 1988, **135**, 2077–2080.
4. RangaRao, G., Fornasiero, P., Dimonte, R., Kaspar, J., Vlaic, G., Balducci, G., Meriani, S., Gubitosa, G., Cremona, A. and Graziani, M., Reduction of NO over partially reduced metal-loaded CeO_2–ZrO_2 solid solutions. *J. Catal.*, 1996, **162**, 1–9.
5. Panhans, M. A. and Blumenthal, R. N., A thermodynamic and electrical conductivity study of nonstoichiometric cerium dioxide. *Solid State Ionic*, 1993, **60**(4), 279–298.
6. Durán, P., Moure, C. and Jurado, J. R., Sintering and microstructural development of Ceria-gadolinia dispersed powders. *J. Mater. Sci.*, 1994, **29**, 4975–4983.
7. Chen, P. L. and Chen, I. W., Reactive cerium (IV) oxide powders by the homogeneous precipitation method. *J. Am. Ceram. Soc.*, 1993, **76**(6), 1577–1583.
8. Zhon, Y. C., Philips, R. J. and Switzer, J. A., Electrochemical synthesis and sintering of nanocrystalline cerium (IV) oxide powders. *J. Am. Ceram. Soc.*, 1995, **78**(4), 981–985.
9. Hirano, M. and Kato, E., Hydrothermal synthesis of cerium (IV) oxide. *J. Am. Ceram. Soc.*, 1996, **79**(3), 777–780.
10. Hirano, M. and Kato, E., Hydrothermal synthesis of nanocrystalline cerium (IV) oxide powders. *J. Am. Ceram. Soc.*, 1999, **82**(3), 786–788.
11. Nakane, S., Tachi, T., Yoshinaka, M., Hirota, K. and Yamaguchi, O., Characterization and sintering of reactive cerium (IV) oxide powders prepared by the hydrazine method. *J. Am. Ceram. Soc.*, 1997, **80**(12), 3221–3224.
12. Chen, P. L. and Chen, I. W., Sintering of fine oxide powders: I, Microstructural evolution. *J. Am. Ceram. Soc.*, 1996, **79**(12), 3129–3141.
13. Chen, P. L. and Chen, I. W., Sintering of fine oxide powders: II, sintering mechanisms. *J. Am. Ceram. Soc.*, 1997, **80**(3), 637–645.
14. Pechini, M. P., *Method of Preparing Lead and Alkaline Earth Titanates and Niobates and Casting Methods Using the Same to Form a Capacitor*. US Patent No. 3.330.697, 11 July 1967.
15. Kakihana, M. and Yoshimura, M., Synthesis and characteristics of complex multicomponent oxides prepared by polymer complex method. *Bull. Chem. Soc. Japn.*, 1999, **72**, 1427–1443.
16. Yamamoto, S., Kakihana, M. and Kato, S., A polymer complex solution route to the low temperature synthesis of tetragonal ZrO_2–CeO_2 with reduced amount of organic substance. *J. Alloys Comp.*, 2000, **297**, 81–86.
17. Uekawa, N., Kakegawa, K. and Sasaki, Y., Synthesis of La-doped lead magnesium niobate by oxidation of polyethylenglycol-cation complex. *J. Ceram. Soc. Jpn.*, 2000, **108**(4), 387–391.
18. Durán, P., Capel, F., Tartaj, J. and Moure, C., Sintering behavior and electrical properties of nanosized doped-ZnO powders produced by metal-organic polymer processing. *J. Am. Ceram. Soc.*, 2001, **84**(8), 1661–1668.
19. Roosen, A. and Bowen, H. K., Influence of various consolidation techniques on the green microstructure and sintering behaviour of alumina powder. *J. Am. Ceram. Soc.*, 1988, **71**, 970–977.
20. Roosen, A. and Hausner, H., Sintering kinetics of ZrO_2 powders. In *Advances in Ceramics, Vol. 12, Science and Technology of Zierconia II*, ed. N. Claussen, M. Ruhle and A. Heuer. American Ceramics Society, Columbus, OH, 1984, pp. 714–726.
21. Fang, T. T. and Palmour, H. III, Useful extensions of statistical theory of sintering. *Ceram. Int.*, 1989, **15**, 329–335.
22. Barringer, E. A. and Bowen, H. K., Formation packing, and sintering of monodispersed TiO_2 powders. *J. Am. Ceram. Soc.*, 1982, **62**(12), C–199-C-201.
23. Hsieh, H. L. and Fany, T. J., Effects of powder processing on the green compacts of high-purity $BaTiO_3$. *J. Am. Ceram. Soc.*, 1989, **72**(1), 142–145.
24. Brook, R. J. In *Concise Encyclopedia of Advanced Ceramic Materials*, ed. R. J. Brook, Pergamon Press, 1991, p.1.
25. Kingery, W. D., Bowen, H. K. and Uhlmann D. R., *Introduction to Ceramics*, 2nd edn. John Wiley Sons, New York, 1976, pp. 486.
26. Hahn, H., Logas, J. and Averback, R. S., Sintering characteristics of nanocrystalline TiO_2. *J. Mater. Res.*, 1990, **5**, 609–614.
27. Sacks, M. D. and Tseng, T. Y., Preparation of SiO_2 Glass from model powders compacts: II, Sintering. *J. Am. Ceram. Soc.*, 1984, **672**, 532–537.